

**Title:**

The Response Of Particles With Anisotropic Shape Within An Optical Landscape And Laminar Flow

**Authors:**

Brandon L. Conover and Michael J. Escuti

**Affiliation:**

North Carolina State University, Dept Electrical & Computer Engineering, Raleigh, NC (USA)

**Presented At:**

*SPIE Optics & Photonics Conference*, San Diego, CA (August 13-17, 2006)

**Citation:**

B.L. Conover and M.J. Escuti, "The Response Of Particles With Anisotropic Shape Within An Optical Landscape And Laminar Flow", *Proceedings of SPIE*, vol. **6326**, no. 632614 (2006).

Copyright 2006 Society of Photo-Optical Instrumentation Engineers.

This paper was published in Proceedings of SPIE Vol. 6326 and is made available as an electronic reprint with permission of SPIE. One print or electronic copy may be made for personal use only. Systematic or multiple reproduction, distribution to multiple locations via electronic or other means, duplication of any material in this paper for a fee or for commercial purposes, or modification of the content of this paper are prohibited.

# The response of particles with anisotropic shape within an optical landscape and laminar flow

Brandon L. Conover and Michael J. Escuti

North Carolina State Univ, Dept Electrical & Computer Engineering, Raleigh, NC (USA)

## ABSTRACT

We have developed an order of magnitude model for the the complete motion—translation and rotation—of spheroidal microparticles under the influence of intense optical landscapes and laminar flow using force and torque balances within the system. Our fields of interest are periodic interference profiles, sometimes termed optical landscapes, that can be formed by simple holography. When given an arbitrary landscape, our model predicts that, in general, spheroidal particles become trapped at a lower potential threshold than do spherical particles of an equivalent volume. In addition, we show that optical landscapes exhibit exponential trapping selectivity based on particle size *and shape*, effectively adding a further dimension of control over which to trap, influence, and sort particles within the same flow.

**Keywords:** Optical Trapping, Optical Manipulation, Optical Tweezers, Microfluidics, Optical Landscape

## 1. INTRODUCTION

The potential to selectively trap, sort, mix, align, and order nano- and micro-scale particles using optical tweezers has become progressively more enhanced in recent years and, as such, have found several uses by themselves and as the backbone of larger systems.<sup>1-4</sup> A sampling of the optical trapping literature finds applications including sorting and manipulation using a diode laser bar to form a large trapping zone,<sup>5</sup> using computer-generated holograms to create arbitrary configurations of single optical traps—sometimes referred to as “holographic optical trapping”,<sup>6,7</sup> deflecting particle trajectories and trapping them in patterns using regular arrays of optical traps,<sup>8,9</sup> creating mult-dimensional optical lattices via the interference of one or more optical beams to sort a flow of particles,<sup>10</sup> and combining parallel optical traps with dielectrophoresis to create optical conveyor belts.<sup>11</sup> On the whole, such methods provide simple reconfiguration of traps being that they are optically formed, in contrast to sorting and manipulation systems that utilize micromachined arrays of obstacles<sup>12</sup> or fluorescence of the particles themselves.<sup>13</sup>

While many of the particles of interest for this type of manipulation are shaped like disks and rods (e.g. blood cells, nanowires, etc) in addition to spheres, many of the theoretical models developed to date focus on single aspects of the system: optical forces exerted on spherical particles under flow within periodic optical landscapes<sup>14,15</sup> or optical torques transferred to ellipsoidal particles within gaussian intensity fields.<sup>16,17</sup> No satisfactory theoretical model has yet been presented that that addresses both the optical forces and optical torques on ellipsoidal particles in a microfluidic flow in order to accurately predict ellipsoidal and spherical particle motion simultaneously.

In this vein, we have developed and derived an order-of-magnitude approximation of the impact of optical force and torque on isotropic dielectric microscale particles with an arbitrary spheroidal shape (prolate, oblate, and spherical) under uniform laminar flow. We avoid calculation of the Maxwell stress tensor or optical scattering by focusing solely on force and torque balance within the system. Our optical fields of interest are primarily one- and two-dimensional periodic interference landscapes formed by simple holography.

A primary prediction of our model is that highly selective trapping into the bright fringes can be accomplished based on shape and volume, in addition to size as previously theorized<sup>14</sup> and demonstrated.<sup>10</sup> In general, we may say that elliptically shaped particles have a trapping threshold that is significantly lower (i.e. easier) than that of spherical particles with an equivalent volume. Additionally, our model also finds that the long axis of

---

Correspondence should be addressed to: mjescuti@ncsu.edu, +1 919 513 7363

any trapped elliptical particle will align into the lowest-energy orientation dictated by the shape of the optical landscape—a property previously theorized<sup>18</sup> and demonstrated in practice using ellipsoidal beams.<sup>19</sup>

While all of the work prior to ours has greatly progressed the field, we have taken the next step in creating a more generalized model applicable to myriad particle shapes and sizes. Our description of the optical torque on microparticles is not only more straightforward to implement than previous attempts but also may be applied to many other systems in which dielectric particles are used. Here we provide the derivation of our model and present several results confirmable by previous physical work by other labs.

## 2. DEVELOPMENT OF PARTICLE MOTION MODEL

A complete model of spheroidal particle motion within a microfluid due to a driving force is satisfied simply by describing the translational motion. Due the laminar flow of the microfluid, rotation does not occur, assuming the particle encounters no forces other than the driving force of the fluid. Once optical forces are present in the system, rotation can occur, owing to torques imparted by the optical fields. Therefore, because we choose optical interference landscapes to influence particle trajectory within the microfluid, a complete model of their motion must now include rotation.

We satisfy these preliminary requirements using two basic hydrodynamic equations capable of determining spheroidal particle position and orientation within the system: force and torque balance equations. Here we now outline the general forms of these equations, the impact of viscous drag on the particles, and the derivations of optically induced force and torque.

### 2.1. Hydrodynamic Balance Equations

Beginning with the Langevin equation of particle motion, the hydrodynamic force balance equation may be derived. Such has been solved and published previously describing spherical particle motion in one-dimension considering stochastic processes (such as Brownian motion) by Risken<sup>20</sup> and in two-dimensions considering potential “landscapes” generated via optical interference by Pelton, Ladavac, and Grier.<sup>14</sup> Both neglected, as do we, inertial effects due to the microfluidic environment (valid when the Reynolds number is  $\ll 1$ ). However, we take the derivation one step further and consider general spheroidal particles, e.g. ellipsoids. Thus, considering viscous flow and drag, stochastic and optical forces, and spheroidal shape, the particle trajectory is described by

$$\overleftrightarrow{\xi}[\Omega] \frac{d\mathbf{r}}{dt} = \mathbf{F}[\mathbf{r}, \Omega] + \mathbf{F}_0 + \mathbf{H}_T[t], \quad (1)$$

where  $\overleftrightarrow{\xi}$  is the translational viscous drag coefficient tensor,  $\mathbf{F}[\mathbf{r}]$  is the spatially-varying optical force field,  $\mathbf{F}_0$  is a uniform driving force in the medium, and  $\mathbf{H}_T[t]$  describes stochastic processes. The vector  $\mathbf{r} = (x, y, z)$  denotes the particle position.

For spherical particles, this force balance equation would be sufficient to describe particle motion. In order to remain general, however, we must take into account the optical torques imparted by optical interference landscapes. The resultant hydrodynamic torque balance equation is derived from first principles and is implemented to describe particle orientation at any point in its trajectory. Considering viscous flow and drag, stochastic and optical torques, and spheroidal shape, particle orientation is described by

$$\overleftrightarrow{\gamma}[\Omega] \frac{d\Omega}{dt} = \mathbf{M}[\mathbf{r}, \Omega] + \mathbf{H}_R[t], \quad (2)$$

where  $\overleftrightarrow{\gamma}$  is the rotational drag coefficient tensor,  $\Omega$  is the angle vector (between the symmetry axis of the particle and the coordinate axes),  $\mathbf{M}[\mathbf{r}]$  is the spatially-varying optical torque field, and  $\mathbf{H}_R[t]$  describes stochastic processes. Note that no flow-induced torque is present owing to uniform laminar flow in the microfluidic environment. The torque balance equation becomes zero should the particle become spherical, reducing the system to that of Pelton.<sup>14</sup>

## 2.2. Viscous Drag Coefficients

Considering a sphere of radius  $a$  submerged in a microfluid of viscosity  $\eta$ , the translational drag coefficient tensor reduces to a scalar and is widely represented by  $\xi = 6\pi\eta a$ . However, because our work focuses on non-spherical particles, the drag depends not only on particle size, but also shape and orientation. Therefore, the translational drag coefficient must be represented as a tensor. Such has been developed for spheroidal particles in the low Reynold's number regime<sup>21</sup> by solving the Navier-Stoke's equation, thus yielding

$$\overleftrightarrow{\xi} = 6\pi\eta \overleftrightarrow{R}, \quad (3)$$

where  $\overleftrightarrow{R}$ , a tensor of rank three with dimension of length, is the hydrodynamic “effective radius” of the spheroidal particle. It is determined by the particle's shape, symmetry (prolate or oblate), and axial dimensions,  $a_u$ .

We note that the rotational drag coefficient,  $\gamma$ , is similar to the translational drag coefficient,  $\xi$ , of the force balance equation in its tensor notation requirement due to particle shape and orientation dependence. A similar equation for the rotational drag has also been developed using the Navier-Stokes equation and an effective radius as before,<sup>22</sup> resulting in

$$\overleftrightarrow{\gamma} = 8\pi\eta \overleftrightarrow{R}^3. \quad (4)$$

## 2.3. The Optically Induced Force and Torque

The spatially-varying force field of Equation (1) has previously been represented<sup>14</sup> as the impact of the optical interference field on a particle. Using our notation, this optically induced force is

$$\mathbf{F}[\mathbf{r}, \Omega] = \int d\mathbf{F} d^3x = -\nabla V[\mathbf{r}, \Omega], \quad (5)$$

where  $V[\mathbf{r}, \Omega]$  represents the force potential,

$$V[\mathbf{r}, \Omega] = (f \circ I)[\mathbf{r}, \Omega]. \quad (6)$$

The particle's form factor,  $f[\mathbf{r}, \Omega]$ , describes its interaction with the periodic optical interference landscape,  $I[\mathbf{r}]$ . Thus, the analytical form for the spatially-varying optical force field may be described, allowing for a solution to the translational motion of spheroidal particles within an optical interference landscape. However, no orientation-related information can be ascertained with this force alone.

In pursuit of a full description of motion for spheroidal particles, we have developed an analytical form for the spatially-varying optical torque field—a feat previously unpublished to any satisfactory degree. We offer that the spatially-varying torque field is a result of the optical interference field imparting a rotating force at a distance  $\mathbf{x}$  from the particle position  $\mathbf{r}$ , yielding

$$\mathbf{M}[\mathbf{r}, \Omega] = \int ((\mathbf{x} - \mathbf{r}) \times d\mathbf{F}) d^3x = \nabla \times \mathbf{A}[\mathbf{r}, \Omega], \quad (7)$$

where  $\mathbf{A}[\mathbf{r}, \Omega]$  represents the torque potential,

$$\mathbf{A}[\mathbf{r}, \Omega] = -(\mathbf{r}f \circ I)[\mathbf{r}, \Omega]. \quad (8)$$

We may now determine both position and orientation for a spheroidal particle in a microfluidic flow under the influence of an optical interference landscape.

## 2.4. Form Factors and Coordinate Systems

Two coordinate systems are needed to represent the particle at any given location: a local (prime) system in which the primary axis,  $a_1$ , lies along the  $\hat{x}'$ -direction and the two equal axes,  $a_2$  and  $a_3$ , lie along the  $\hat{y}'$ - and  $\hat{z}'$ -directions, respectively; and a global system in which the orientation of the particle may be any angle,  $\Omega$ . These systems share an origin at which the position vectors  $\mathbf{r}$  and  $\mathbf{r}'$  are anchored. Both are represented

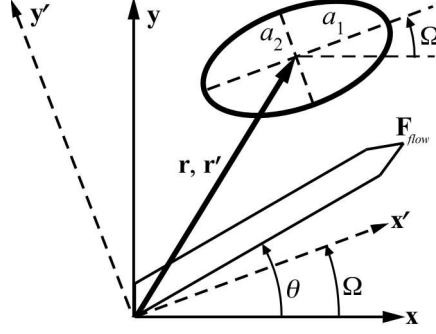


**Figure 1.** Coordinate systems used to represent a spheroidal particle at orientation  $\Omega$  and position  $\mathbf{r}, \mathbf{r}'$ .

graphically in Fig. 1. The driving force,  $\mathbf{F}_{flow}$ , exists in both the global and local systems, at angles of  $\theta$  and  $\theta - \Omega$ , respectively.

The final piece in our derivation of the force and torque balance equations is a description of the form factors,  $f[\mathbf{r}]$ , present in both Eqns. (6) and (8). Allowing the particle to exist within a periodic optical interference landscape, we may represent the form factor in local coordinates as

$$f[\mathbf{r}'] = \alpha \sqrt{a_1 a_2} \exp \left\{ -\frac{x'^2}{2a_1^2} - \frac{y'^2}{2a_2^2} \right\}, \quad (9)$$

and in global coordinates as

$$f[\mathbf{r}, \Omega] = \alpha \sqrt{a_1 a_2} \exp \left\{ -\frac{(x \cos \Omega + y \sin \Omega)^2}{2a_1^2} - \frac{(-x \sin \Omega + y \cos \Omega)^2}{2a_2^2} \right\}, \quad (10)$$

by simply applying the appropriate rotation transformations. In both cases,  $\alpha$  represents the particle's polarizability. Using the Fourier Convolution Theorem,

$$(f \circ I)[\mathbf{r}, \Omega] = \mathcal{F}^{-1} \{ \tilde{f}[\mathbf{k}'] \tilde{I}[\mathbf{k}', \Omega] \}, \quad (11)$$

we can take the Fourier transforms of  $f$  and  $I$  individually being that each is a separable equation. Since  $I$  may represent any unique landscape, its Fourier transform,  $\tilde{I}$ , changes accordingly. The form factor, however, remains constant as does its Fourier transform,

$$\tilde{f}[k'_x, k'_y] = 2\pi \alpha a_1 a_2 \sqrt{a_1 a_2} * \exp(-2\pi^2 a_1^2 k_x'^2) \exp(-2\pi^2 a_2^2 k_y'^2). \quad (12)$$

We now possess all required information to begin implementing our model to make an approximation of particle motion within given optical interference landscapes.

### 3. IMPLEMENTATION OF PARTICLE MOTION MODEL

In order to exhibit the quality and relevance of our model, we now present results implementing both one-dimensional and two-dimensional sinusoidal optical interference landscapes. Such landscapes can be formed via simple holography and, thus, are realistic and valuable to model.

#### 3.1. 1D Sinusoidal Optical Interference Landscapes

The 1D sinusoidal optical interference landscape varies only in the  $\hat{x}$ -direction so that  $I[x]$  is symmetrical in the  $\hat{y}$ -direction. Such is represented as

$$I[x] = I_0 \left( 1 + \cos \left( \frac{2\pi}{\Lambda_x} x \right) \right), \quad (13)$$

where  $\Lambda_x$  is the interference pitch. We first must find  $\tilde{I}$  and take the product of it and the proper form factor construction, Eq. (12), in order to implement Eq. (11) and solve for the force and torque potentials (Eqs. (6) and (8)). In component form, the optical force, Eq. (5), and optical torque, Eq. (7), become

$$F_{x'}[x', y', \Omega] = 2\pi I_0 \left\{ \frac{\cos \Omega}{\Lambda_x} \tilde{f} \left( \frac{\cos \Omega}{\Lambda_x}, \frac{\sin \Omega}{\Lambda_x} \right) \sin \left( \frac{2\pi}{\Lambda_x} (x' \cos \Omega - y' \sin \Omega) \right) \right\} \quad (14a)$$

$$F_{y'}[x', y', \Omega] = -2\pi I_0 \left\{ \frac{\sin \Omega}{\Lambda_x} \tilde{f} \left( \frac{\cos \Omega}{\Lambda_x}, \frac{\sin \Omega}{\Lambda_x} \right) \sin \left( \frac{2\pi}{\Lambda_x} (x' \cos \Omega - y' \sin \Omega) \right) \right\} \quad (14b)$$

$$M[x', y', \Omega] = 4\pi^2 I_0 \left\{ -\frac{\sin \Omega \cos \Omega}{\Lambda_x^2} (a_1^2 - a_2^2) \tilde{f} \left( \frac{\cos \Omega}{\Lambda_x}, \frac{-\sin \Omega}{\Lambda_x} \right) \cos \left( \frac{2\pi}{\Lambda_x} (x' \cos \Omega - y' \sin \Omega) \right) \right\}. \quad (14c)$$

Before we are able to solve the force and torque balance equations, however, we must define the driving force term,  $\mathbf{F}_0$ , as well as determine the form of the stochastic forces. Because we are examining a case of particle response to microfluidic flow, we will allow stochastic forces to be negligible in relation to the other forces present. We use the force of microfluidic flow to be the driving force, represented graphically by  $\mathbf{F}_{flow}$  in Fig. 1, and represented analytically by

$$\mathbf{F}_{flow} = \overleftrightarrow{\xi} \mathbf{v}_0, \quad (15)$$

where the vector  $\mathbf{v}_0$  is the flow velocity.

We now choose to solve the force and torque balance equations in differential form. The force balance equation, Eq. (1), as differential components including the corresponding microfluidic flow terms is expressed as

$$\frac{dx'}{dt} = \frac{1}{\xi_{x'}[\Omega]} F_{x'}[x', y', \Omega] + v_0 \cos \theta \quad (16a)$$

$$\frac{dy'}{dt} = \frac{1}{\xi_{y'}[\Omega]} F_{y'}[x', y', \Omega] + v_0 \sin \theta. \quad (16b)$$

It is important to note that there is no driving force term within the torque balance equation, Eq. (2), due to the laminar flow condition. Therefore, it will be used in the following differential form:

$$\frac{d\Omega}{dt} = \frac{1}{\gamma} M[x', y', \Omega]. \quad (17)$$

We now have analytical expressions describing the complete spheroidal particle motion influenced by a 1D optical landscape within a microfluidic flow environment. The most exciting result of simulating this motion is that we show *a very high selectivity among spheroidal particle types in trapping threshold*, most notably that elliptical particles are much easier to trap within the optical landscape, i.e. it takes less optical power to influence and trap oblate and prolate particles than it does spherical particles.

This may be illustrated in several ways, the first of which is shown in Fig. 2, a rendering of particle orientation and trajectory for each shape given a specific normalized potential. The normalized potential has units of inverse volume and generalizes the data for interference pitch, optical intensity, viscous drag, particle polarizability, and the driving force. One may note the differences among the particle types: the sphere moves directly with the microfluidic flow (the dashed line at  $\frac{\pi}{9}$ ), the oblate particle is immediately trapped, and the prolate particle has a varying trajectory as it passes each bright fringe.

In an effort to further visualize the variation in trapping potential for the three particle types, Fig. 4 plots the normalized minimum potential necessary to trap a particle in a single bright fringe of the optical interference landscape based on particle ellipticity,

$$ellipticity = 1 - \frac{a_2^2}{a_1^2}, \quad (18)$$

a unitless parameter. Each line represents a certain volume. Lower normalized potential values equate to easier trapping ability. For the smaller volumes, the sphere (*ellipticity* = 0) requires the highest potential to trap while

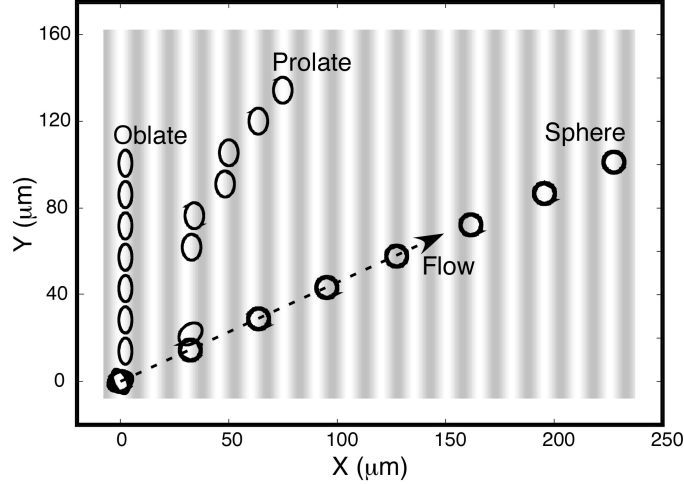


**Figure 2.** Individual particle movement in a laminar flow for a specific normalized potential within a 1D optical landscape. The volume of each particle is  $250 \mu\text{m}^3$ . The interference pitch,  $\Lambda_x$ , is  $15 \mu\text{m}$  and the flow velocity,  $v_0$ , is  $9 \frac{\mu\text{m}}{\text{s}}$  at a flow angle,  $\theta$ , of  $\frac{\pi}{9}$ . The intensity,  $I_0$ , is on the order of  $5 \frac{\text{MW}}{\text{m}^2}$ .

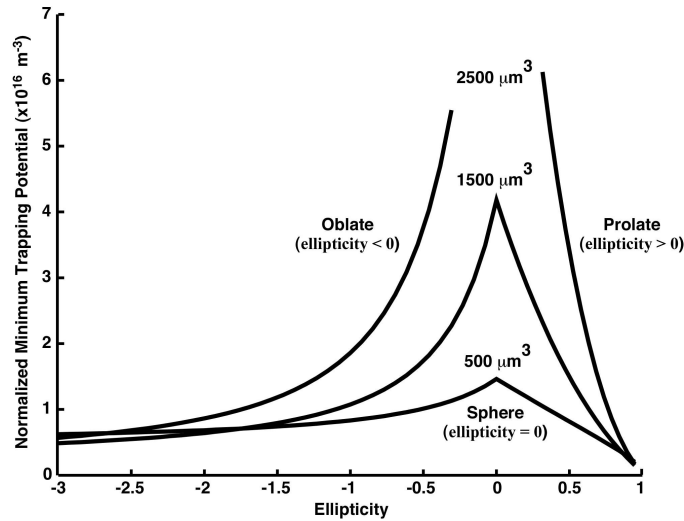


**Figure 3.** Normalized minimum potential necessary to trap various elliptical particles of varying volume.

at the higher volume, the sphere as well as particles approaching spherical are not trappable at any potential. It is interesting to note that at ellipticities far from spherical, the normalized potential values begin to merge, i.e. highly elliptical particles are easy to trap regardless of their volume.

For Fig. 4, we have chosen a single case of specific particle ellipticities (-2, 0, +0.5) possessing an equivalent volume ( $250 \mu\text{m}^3$ ) and plot how each behaves based on the normalized potential of the system. We use the parameter  $\tan(\Psi)$  in an effort to show results in comparison with Pelton.<sup>14</sup> The angle,  $\Psi$ , is measured from the y axis of the global coordinate system, i. e.  $\Psi = 0$  at  $y = 0$ , and extends to the angle of flow, in this case  $\Psi = \frac{\pi}{9}$ . Along the horizontal axis of the plot,  $\tan(\Psi)$  is zero and the particle is trapped in a bright fringe. At the dashed line, the particle moves in the same direction as the microfluidic flow, uninfluenced by the optical interference landscape. Between these two extremes, the particle's trajectory is altered by the landscape, but not enough to cause complete trapping.

At this point, we must draw attention to another of our major findings and verification of our model's accuracy: *elliptical particles will align themselves to the bright fringes in their minimum energy configuration.*

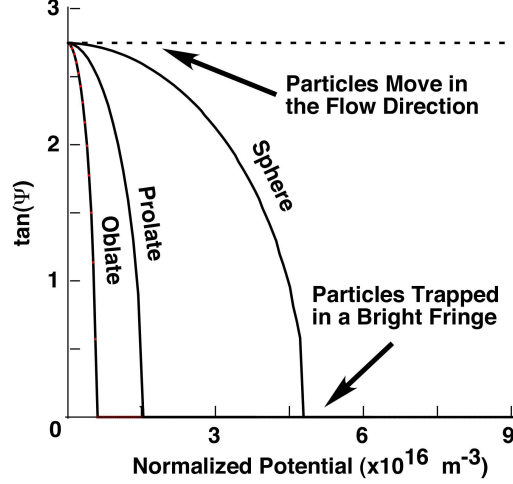


**Figure 4.** Averaged trajectory ( $\tan(\Psi)$ ) of three particle types in a laminar flow and a 1D optical landscape for various normalized potentials. The volume of each particle is  $250 \mu m$ .

For prolate particles, the major axis is aligned parallel with the bright fringe while, for oblate particles, the major axis is aligned perpendicular with the bright fringe. In effect, the particles tend to fit as much of their volume within the bright fringe as possible. In Fig. 2, this is immediately apparent, and while the prolate particle's orientation may vary at first, and while its position in the x-y plane is changing, it quickly aligns itself in the minimum energy configuration. For the sphere, there is no minimum energy configuration because all are equivalent.

### 3.2. 2D Sinusoidal Optical Interference Landscapes

The 2D sinusoidal optical interference landscape varies in both the  $\hat{x}$ - and the  $\hat{y}$ -directions with identical or dissimilar interference pitch values. We represent this landscape as

$$I[x, y] = \left( 1 + \cos\left(\frac{2\pi}{\Lambda_x} x\right) + \cos\left(\frac{2\pi}{\Lambda_y} y\right) \right). \quad (19)$$

We must again find  $\tilde{I}$  and work our way to the component forms of optical force and torque,

$$F_{x'}[x', y', \Omega] = 2\pi I_0 \left\{ \frac{\cos \Omega}{\Lambda_x} \tilde{f}\left(\frac{\cos \Omega}{\Lambda_x}, \frac{\sin \Omega}{\Lambda_x}\right) \sin\left(\frac{2\pi}{\Lambda_x} (x' \cos \Omega - y' \sin \Omega)\right) + \frac{\sin \Omega}{\Lambda_y} \tilde{f}\left(\frac{\sin \Omega}{\Lambda_y}, \frac{\cos \Omega}{\Lambda_y}\right) \sin\left(\frac{2\pi}{\Lambda_y} (x' \sin \Omega + y' \cos \Omega)\right) \right\} \quad (20a)$$

$$F_{y'}[x', y', \Omega] = -2\pi I_0 \left\{ \frac{\sin \Omega}{\Lambda_x} \tilde{f}\left(\frac{\cos \Omega}{\Lambda_x}, \frac{\sin \Omega}{\Lambda_x}\right) \sin\left(\frac{2\pi}{\Lambda_x} (x' \cos \Omega - y' \sin \Omega)\right) + \frac{\cos \Omega}{\Lambda_y} \tilde{f}\left(\frac{\sin \Omega}{\Lambda_y}, \frac{\cos \Omega}{\Lambda_y}\right) \sin\left(\frac{2\pi}{\Lambda_y} (x' \sin \Omega + y' \cos \Omega)\right) \right\} \quad (20b)$$

$$M[x', y', \Omega] = -4\pi^2 I_0 \sin \Omega \cos \Omega (a_1^2 - a_2^2) \left\{ \frac{1}{\Lambda_x^2} \tilde{f}\left(\frac{\cos \Omega}{\Lambda_x}, \frac{-\sin \Omega}{\Lambda_x}\right) \cos\left(\frac{2\pi}{\Lambda_x} (x' \cos \Omega - y' \sin \Omega)\right) + \frac{1}{\Lambda_y^2} \tilde{f}\left(\frac{\sin \Omega}{\Lambda_y}, \frac{\cos \Omega}{\Lambda_y}\right) \cos\left(\frac{2\pi}{\Lambda_y} (x' \sin \Omega + y' \cos \Omega)\right) \right\}. \quad (20c)$$

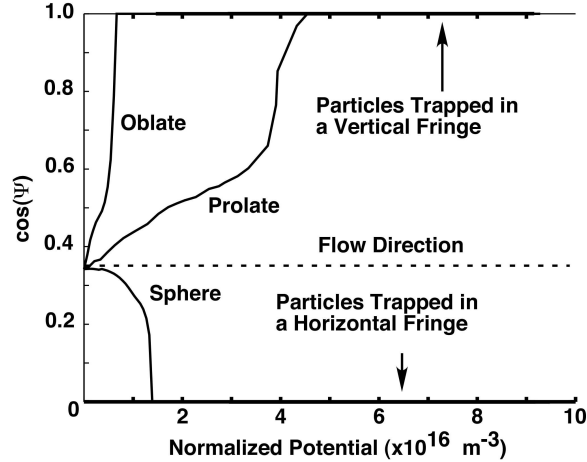


**Figure 5.** Averaged trajectory ( $\cos(\Psi)$ ) of three particle types in a laminar flow and a 2D optical landscape for various normalized potentials. The volume of each particle is  $1500 \mu\text{m}$ .

The differential components are found in much the same manner as before as we choose to keep the same form for the driving force.

The most striking result of this landscape's influence is the many trajectories available to particles depending on their type and on the normalized potential of the system. Fig. 5, as in Fig. 4 for the 1D case, illustrates a form of particle trajectory as a function of the normalized potential. However,  $\tan(\Psi)$  is no longer a valid parameter because the trajectory may be any value between 0 and  $\pi/2$ . Therefore, we have chosen to use  $\cos(\Psi)$ . In a steady state condition, with  $\Lambda_x = \Lambda_y$ , the oblate and prolate particles become trapped in a vertical fringe while the spherical particle prefers the horizontal fringe. Note that no particle follows the flow direction. However, by simply altering the interference pitch values, one has very selective control over which fringe, if any, will trap a certain particle.

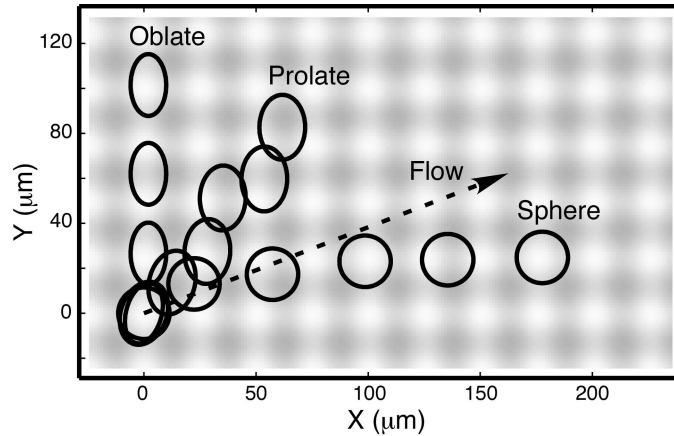
Also of interest in Fig. 5 is that the prolate particle requires higher potentials to trap than the spherical particle. This is in contrast to both the 1D case in which the spherical particle required the highest potential to become trapped and to previously published results<sup>14</sup> stating there is no qualitative difference in 2D modulation of separable landscapes. We attribute the first to a fundamental change in landscape representation from extended lines of traps to a parallel array of traps exerting a very different influence on spheroidal particles. Our model does agree with the previous results in terms of the spherical particle, but we do find a very noticeable difference in general spheroidal particle behavior in the 2D modulated case.

Fig. 6, much like Fig. 2, shows how the various particle types change their orientations and trajectories for a specific normalized potential within a 2D optical landscape. A potential has been selected in which the spherical particle is trapped before the prolate particle as discussed above. All particles possess a volume of  $1500 \mu\text{m}$  and the two interference pitch values are equivalent.

#### 4. CONCLUSIONS AND CURRENT WORK

We have described the complete motion of spheroidal microparticles in a microfluidic laminar flow influenced by optical interference landscapes within a model of optical force and torque balance equations. Our work has expanded on others' including Pelton, Ladavac and Grier<sup>14</sup> to which our model reduces when all particle axes are equal (spherical) and with which our analytical data is comparable in the spherical regime.

Our major achievement is the full derivation of the optical torque balance equation in conjunction with the optical force balance equation previously defined.<sup>14</sup> By uniting these equations into one analytical model, we have been able to predict the behavior of spheroidal particle orientation with the optical interference fringes and highlight the exponential sensitivity to shape. We also predict orientational behavior in 1D and 2D optical



**Figure 6.** Averaged trajectory ( $\cos(\Psi)$ ) of three particle types in a laminar flow and a 2D optical landscape. The volume of each particle is  $1500 \mu\text{m}^3$ . The interference pitch values,  $\Lambda_x$  and  $\Lambda_y$ , are both  $25 \mu\text{m}$ . The flow velocity,  $\mathbf{v}_0$  is  $9 \frac{\mu\text{m}}{\text{s}}$  at a flow angle,  $\theta$ , of  $\frac{\pi}{9}$ . The intensity,  $I_0$ , is on the order of  $7 \frac{\text{MW}}{\text{m}^2}$ .

lattices with some similarities to the work of Rockstuhl,<sup>16</sup> in which elliptical cylinders inside a single trap were analyzed.

In an effort to provide physical verification of our modeling work, we are forming our own optical landscapes by interfering optical beams produced a Nd:YAG laser operating at 1064 nm. Our particles of interest include microscale glass rods (prolate particles), latex microspheres (spherical particles), and red blood cells (oblate particles). It is our intent to show a system in which several particle types may be sorted or trapped based on size and shape for various applications, including “lab-on-a-chip” integration and massively parallel arrangements of cells.

## REFERENCES

1. A. Ashkin, “Optical trapping and manipulation of neutral particles using lasers,” *Proc. Natl. Acad. Sci. USA* **94**, pp. 4853–4860, 1997.
2. D. G. Grier, “A revolution in optical manipulation,” *Nature* **424**, pp. 810–816, 2003.
3. K. Dholakia, G. Spalding, and M. MacDonald, “Optical tweezers: the next generation,” *Physics World*, pp. 31–35, 2002.
4. J. Enger, M. Goksor, K. Ramser, P. Hagberg, and D. Hanstorp, “Optical tweezers applied to a microfluidic system,” *Lab Chip* **4**, pp. 196–200, 2004.
5. R. W. A. Jr., J. Squier, T. Vestad, J. Oakey, and D. W. M. Marr, “Optical trapping, manipulation, and sorting of cells and colloids in microfluidic systems with diode laser bars,” *Opt. Exp.* **12**(19), pp. 4390–4398, 2004.
6. P. T. Korda, M. B. Taylor, and D. G. Grier, “Kinetically locked-in colloidal transport in an array of optical tweezers,” *Phys. Rev. Lett.* **89**(12), 2002.
7. D. G. Grier and Y. Roichman, “Holographic optical trapping,” *App. Opt.* **45**(5), pp. 880–887, 2006.
8. F. C. Cheong, C. H. Sow, A. T. S. Wee, P. Shao, A. A. Bettiol, J. A. V. Kan, and F. Watt, “Optical travelator: transport and dynamic sorting of colloidal microspheres with an asymmetrical line optical tweezers,” *App. Phys. B* **83**, pp. 121–125, 2006.
9. K. Ladavac, K. Kasza, and D. G. Grier, “Sorting mesoscopic objects with periodic potential landscapes: Optical fractionation,” *Phys. Rev. E* **70**, 2004.
10. M. MacDonald, S. Neale, L. Paterson, A. Richies, K. Dholakia, and G. Spalding, “Cell cytometry with a light touch: Sorting microscopic matter with an optical lattice,” *J. Biol. Regul. Homeost. Agents* **18**(2), 2004.
11. P. Y. Chiou, A. T. Ohta, and M. C. Wu, “Massively parallel manipulation of single cells and microparticles using optical images,” *Nature* **436**, pp. 370–372, 2005.

12. J. C. T. Eijkel and A. van den Berg, "The promise of nanotechnology for separation devices—from a top-down approach to nature-inspired separation devices," *Electrophoresis* **27**, pp. 677–685, 2005.
13. D. W. Galbraith, M. T. Anderson, and L. A. Herzenberg, "Flow cytometric analysis and FACS sorting of cells based on GFP accumulation," *Meth. Cell. Bio.* **58**, pp. 315–341, 1999.
14. M. Pelton, K. Ladavac, and D. G. Grier, "Transport and fractionation in periodic potential-energy landscapes," *Phys. Rev. E* **70**, 2004.
15. J. P. Gleeson, J. M. Sancho, A. M. Lacasta, and K. Lindenberg, "Analytical approach to sorting in periodic and random potentials," *Phys. Rev. E* **73**, 2006.
16. C. Rockstuhl and J. Tominaga, "Calculation of the torque exerted by light fields on silver elliptical nanocylinders," *Europhys. Lett.* **73**(2), pp. 313–319, 2006.
17. A. I. Bishop, T. A. Nieminen, N. R. Heckenberg, and H. Rubinsztein-Dunlop, "Optical application and measurement of torque on microparticles of isotropic nonabsorbing material," *Phys. Rev. A* **68**, 2003.
18. C. Rockstuhl and H. P. Herzig, "Calculation of the torque on dielectric elliptical cylinders," *J. Opt. Soc. Am. A* **22**(1), pp. 109–116, 2005.
19. S. K. Mohanty, R. Dasgupta, and P. K. Gupta, "Three-dimensional orientation of microscopic objects using combined elliptical and point optical tweezers," *App. Phys. B* **81**, pp. 1063–1066, 2005.
20. H. Risken, *The Fokker-Planck Equation*, Springer-Verlag, Berlin, 1989 (second edition).
21. T. Ambjörnsson and S. P. Apell, "Ellipsoidal particles driven by intensity gradients through viscous fluids," *Phys. Rev. E* **67**, 2003.
22. L. D. Landau and E. M. Lifshitz, *Fluid Mechanics*, vol. 6 of *Course of Theoretical Physics*, Butterworth-Heinemann, 1998 (second edition).